redin Revista Facultad de Ingeniería, Universidad de Antioquia, No.104, pp. 33-41, Jul-Sep 2022

Effect of the opening and location ratio on the performance of an H-Darrieus VAWT

Efecto de la relación de abertura y ubicación en el rendimiento de una H-Darrieus VAWT

Andrés Burbano-Hernández [1*], **Diego Hincapié** [1], **Jonathan Graciano-Uribe** [1], **Edwar Torres-López** [2]

[1]Departamento de Ingeniería Mecatrónica, Grupo de Investigación MATyER, Instituto Tecnológico Metropolitano. Calle 73 # 76A-354, Vía al Volador. C. P. 050034, Medellín, Colombia.
[2]Departamento de Ingeniería Mecánica, Universidad de Antioquia. Cl. 67 # 53-108. C. P. 050010, Medellín, Colombia.

CITE THIS ARTICLE AS:

A. Burbano, D. Hincapié, J. Graciano and E. Torres. "Effect of the opening and location ratio on the performance of an H-Darrieus VAWT", *Revista Facultad de Ingeniería Universidad de Antioquia*, no. 104, pp. 33-41, Jul-Sep 2022. [Online]. Available: https://www.doi.org/10.17533/udea.redin.20210737

ARTICLE INFO:

Received: October 30, 2020
Accepted: July 16, 2021
Available online: July 16, 2021

KEYWORDS:

H-Darrieus; Airfoil; ratio; CFD; NACA; Efficiency

H-Darrieus; Perfil aerodinámico; Proporción; CFD; NACA; Eficiencia

ABSTRACT: Vertical axis wind turbines such as Darrieus turbines are a very interesting category of low wind speed domestic wind turbines. Further research work is needed to enhance their efficiency to fulfill the higher demand in small applications for power generation. The main objective of this work is to find a Darrieus turbine design to boost the starting capacity of the turbine through an opening located at the lower surface of the airfoil. We carried out a thorough CFD (Computational Fluid Dynamics) investigation to determine the impact of the opening position on the Darrieus rotor's output. This new type of airfoil uses a standard NACA 0015 profile and a profile with an opening on the lower surface of the profile. Different sizes of the opening in a symmetrical profile are evaluated through the CFD method to predict the C_p and C_T of this H-Darrieus turbine design. Five sections were designed to describe the research of this new H-Darrieus rotor. Generally speaking, the results showed that the C_p decreases with the opening ratio, the desirable rotors with the lower surface opening ratio are 0.12 to 0.36 considering this with the low C_pLP.

RESUMEN: Las turbinas eólicas de eje vertical como las turbinas Darrieus son un tipo muy interesante de turbinas eólicas domésticas con bajas velocidades de viento. Se necesita más trabajo de investigación para mejorar su rendimiento a fin de satisfacer la mayor demanda de generación de energía en aplicaciones pequeñas. El objetivo principal de este trabajo es encontrar un diseño de una turbina Darrieus para mejorar la capacidad de arranque de la turbina a través de una abertura situada en la superficie inferior del perfil. Se llevó a cabo una investigación de CFD (Dinámica de Fluidos Computacional) para determinar el impacto de la posición de la abertura en la salida del rotor Darrieus. Este nuevo tipo de perfil aerodinámico utiliza un perfil estándar NACA 0015 y un perfil con una abertura en la superficie inferior del perfil. Los diferentes tamaños de la abertura en un perfil simétrico se evalúan a través del método CFD para predecir el C_p y C_T de este diseño de turbina H-Darrieus. Se diseñaron cinco secciones para describir la investigación de este diseño de H-Darrieus. En términos generales, los resultados mostraron que el C_p disminuye con la relación de apertura, los rotores deseables con la relación de apertura son de 0,12 a 0,36 considerando esto con el bajo el criterio de un menor C_pLP.

* Corresponding author: Andrés Burbano-Hernández
E-mail: andresburbano249993@correo.itm.edu.co
ISSN 0120-6230
e-ISSN 2422-2844

1. Introduction

The global contribution of buildings to energy use, both residential and commercial, has gradually risen in developing countries, exceeding figures between 20% and 40%, and has surpassed other primary industries: manufacturing and transport industries. Development in the population, growing demand for housing facilities and comfort levels, and increasing time spent within houses would ensure that the upward rise in energy demand persists in the future [1]. Residential and industrial consumption of energy is increasing at an annual rate of 0.4% to 0.5% per annum from 2018 to 2050 [2], according to the US EIA (Energy Information Administration) evaluation. The use of renewable energies would also be an indicator of a viable future for energy development in houses. In the urban area, small or micro-wind turbines have lately gained more interest. There are some benefits of integrating wind turbines into buildings. The electricity generated by the wind turbine can be fed directly into the building's electrical circuits, which could minimize the expense of linking the distribution network to the local grid and eliminate losses in energy transport. Several efforts have been made to make a structured grouping of wind turbines coordinated, but this provides a slight advantage as their practical utility drastically reduces the number of basic designs. Wind turbines are classified based on their aerodynamic functions, followed by the turbine's configuration and construction. The aerodynamic function of the rotor is defined by whether the wind turbine derives its power primarily from the rotor-acting air stream's aerodynamic drag or whether it is capable of capturing the aerodynamic lift produced by the flow across streamlined bodies. In particular, several attempts have been made in Germany, the US, and the UK to grow and refine this form to commercial maturity. Musgrove (British Engineer) suggested straight blades as H-rotors with variable rotor geometry to control the strength and turbine RPM. However, the cost of this principle is still high as compared with horizontal-axis rotors. The Darrieus H-rotor turbine [3] was developed by a German manufacturer and had features such as a basic structure and a generator, which are directly built into the rotor without using a gearbox.

VAWTs, particularly the Darrieus lift-type rotors, appear to be the most suitable turbines in the building environment because of their unique properties, independent of wind direction, low noise, and vibration intensity. Some studies have shown that in skewed flow and horizontal wind turbines, H-Darrieus produces higher power output but suffers from a decrease in power [4].

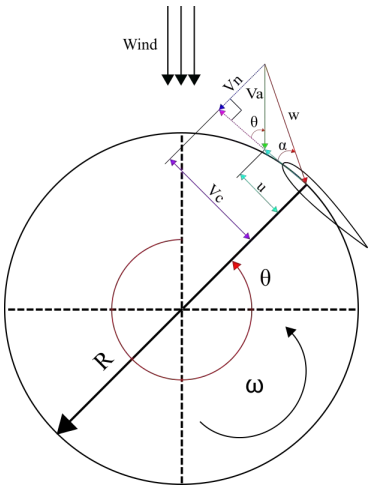

Figure 1 Darrieus turbine airfoil flow velocities

2. Turbine description

The wind flow flows over the turbine blades composed of an airfoil cross-section profile to create beneficial torque and power. A relative velocity W is produced, as with any airfoil, due to a vector difference between absolute wind velocity V_a and peripheral blade velocity u, as shown in Figure 1. The tip speed ratio (TSR) is a ratio of the tip blade velocity ωR to the freestream wind velocity, and this ratio is defined as Equation (1).

$$\lambda = \frac{\omega R}{\vartheta} \tag{1}$$

From the analysis of the velocity triangle (Figure 1), a relation between the attack angle α, the azimuth angle θ, and the tip speed ratio (TSR) λ was defined; this relation is given by Equation (2).

$$a = \tan^{-1}\left[\frac{\sin(\theta)}{\lambda + \cos(\theta)}\right] \tag{2}$$

The relative flow velocity w can be obtained as Equation (3):

$$w = \sqrt{V_C + V_n} \tag{3}$$

Where the chordal velocity component is represented by V_c and the normal velocity component is represented by V_n. The values of the angle of attack with the azimuth angle variance can be estimated from Equation (2), but the crucial factor for defining the geometry of the vertical axis wind turbine is the rotor solidity, which can be determined as Equation (4):

$$\sigma = \frac{Nc}{D} \tag{4}$$

As shown in Equation (4), the solidity is a function of the number of blades N, chord length C of the airfoil, and the diameter D of the rotor.

A Darrieus wind turbine performance is a function of

several parameters, such as wind speed ϑ, mechanical output power P, mechanical torque T on the turbine axis, rotor radius R, fluid density ρ, and turbine height H. In this case, due to 2D analysis, H=1. Through combining these parameters, the torque and power coefficients equation can be obtained and written as follows Equation 5 and Equation 6:

$$C_T = \frac{T}{\rho \vartheta^2 R^2 H} \tag{5}$$

$$C_P = \frac{P}{\rho \vartheta^3 R H} \tag{6}$$

Where C_p and C_T are the torque and power coefficients, respectively. NACA 0015 airfoil [5, 6] is the airfoil being studied. The length of the airfoil's chord is 250 mm, and the turbine radius and height are 1250 mm and 1000 mm, respectively. In Figure 2, the profile of the airfoil NACA 0015 can be seen. Researchers working on airfoil for VAWT applications have suggested three design variations which have been independently shown to optimize airfoil aerodynamics and thus increase the self-starting capacity. First, Hill *et al.* [7] Investigated the self-starting capacity of an H-rotor Darrieus turbine under steady wind conditions using wind tunnel experiments and numerical simulations. The study revealed that a turbine with a solidity of 0.33 would self-start at a uniform freestream velocity of 6 m/s. Second, Dominy *et al.* [8] developed a numerical simulation to determine the parameters that determine the self-starting capability of a Darrieus turbine. The results suggest that a lightly loaded three-bladed rotor always has the potential to self-start under steady fluid conditions. At the same time, the starting of a two-bladed device is dependent on its initial rotor position. The first modification on the airfoil is the Gurney flap, which is a vertical flap.

Gurney flaps have been shown to enhance the lift coefficients of the airfoil through experimental studies [9]. A Gurney flap with a height of 1.25 percent of the airfoil chord length (c) enhances the lift with just a slight improvement in the drag coefficient [9]. This phenomenon is explained in the NACA 0012 [10] airfoil study, which states that the Gurney flap increases the suction of the upper surface of the airfoil and the pressure on the lower surface, which, in effect, increases lift. Outward dimples on the airfoil's upper surface, the second variation, will operate as a vortex generator to enhance the airfoil lift coefficient [11]. These dimples increase the flow turbulence and reduce the wake, thus minimizing the drag coefficient. They help increase the overall lift at a higher AOA (angle of attack). The combined aerodynamic effect has also been shown to influence the angle of the stall. The third modification is an investigation of the NACA-0015 airfoil with both the dimple and the Gurney flap on the inner surface of the tail edge to improve the airfoil's dynamic performance [12]. The study showed an increase in the average tangential force of 35 percent in steady-state and 40 percent in the oscillating case (at each revolution) using a combination of a Gurney flap and a semi-circular inward dimple.

Table 1 Rotor definitions for NACA 0015 airfoil

Opening ratio	Inner (in*)
0	0015-0 (in)
0.12	0015-0.12 (in)
0.24	0015-0.24 (in)
0.36	0015-0.36 (in)
0.48	0015-0.48 (in)
0.60	0015-0.60 (in)
0.72	0015-0.72 (in)
0.84	0015-0.84 (in)

** in corresponds to the inner opening*

In summary, the aforementioned studies provide a basis for the self-starting capacity of VAWTs and geometric modifications in the airfoil, allowing us to create a structured model wherein the turbine is designed by variables such as freestream velocity, solidity, and the number of blades. Furthermore, an opening in the lower part of the airfoil is designed to optimize the geometry of the airfoil and increase the self-starting capacity of the H-Darrieus turbine by reducing the negative C_T presented in the dead zone. Quantitatively, this average C_T value for the dead zone is expected to be greater than 0, if this value is greater than zero (which is already at a value greater than zero since the model was performed with the previously highlighted listed studies), indicates whether the turbine has an excellent self-starting capacity and increasing the C_p along with low TSR values.

In this analysis, the mounting ratio was set to 0 (the chord length's midpoint), defined as the ratio of the chord length's leading point to its mounting point. The opening location and opening ratios are described in Figure 3. For the airfoil used, seven opening ratios of 0.12, 0.24, 0.36, 0.48, 0.60, 0.72, and 0.84 were investigated. The opening ratio corresponds to the ratio between the opening size and the chord length of the airfoil. The opening location corresponds to the opening position, where the opening position is on the lower (inner) surface of the NACA 0015 airfoil. Eight (8) unique opening ratios are shown in Figure 3, where the opening is situated on the inner side. Location and opening ratios without considering the shaft were tested at the same mounting ratio. Each case is given an abbreviation mentioned in Table 1 in order to discuss the simulation results. The C_p and C_T of this rotor are simulated at 10 m/s wind speed applied on the inlet.

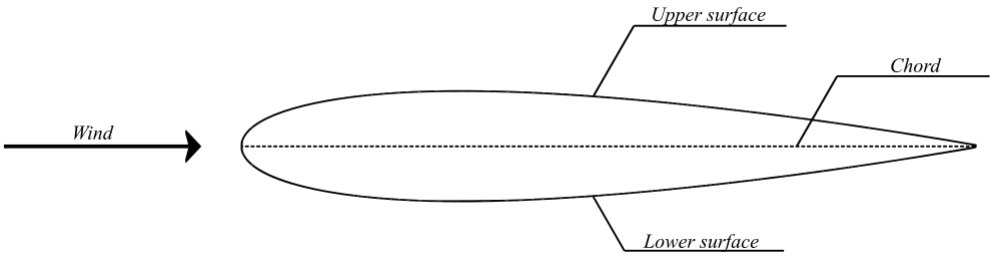

Figure 2 NACA 0015 airfoil

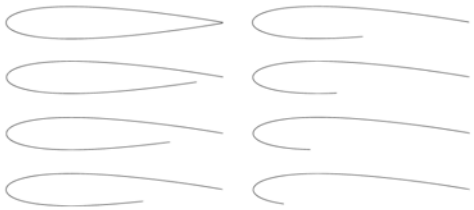

Figure 3 NACA 0015 Design parameters

3. CFD strategy and validation

The Momentum, Vortex, and Cascade are the models widely used for the C_p calculation of the VAWTs. In 2008, Islam [13] listed the advantages and drawbacks of the three approaches. One of the essential tasks of these models is to build the aerodynamic airfoil database [14]. However, it is difficult to find reliable aerodynamic databases with a low Reynolds number range [15] and an entire range, particularly for opening NACA airfoils. Consequently, this new hybrid rotor's performance estimation and examination were carried out using AOA equal to 0. CFD research on VAWTs has received much attention today due to the rapid growth of computational capabilities. Table 2 briefly summarizes the CFD simulations of VAWTs implemented by different authors. Most of them reach a consensus on CFD modeling conditions, including inlet, outlet, domain size, pressure-velocity algorithm, and others. Therefore, based on this summary, ANSYS FLUENT will be used as the solver applying the finite volume method to discretize the governing equations.

Zhang *et al.* [20] predicted drag and lift forces, pressure, and velocity field for a full-scale passenger vehicle with two independent front-end configurations using four RANS models. The models were the realizable $k-\varepsilon$, the AKN, the SST $k-w$, and the V2F [21]. They observed that the realizable $k-\varepsilon$ was better than the other three RANS models for the base model. However, due to its reasonable accuracy, low cost of calculation, and rapid recovery time, the RANS model may still be the right choice for predicting drag values. Although the drag coefficient is not the most appropriate parameter for an in-depth study of this proposed model, the lift coefficient is one of the parameters that attracts attention to H-Darrieus turbines because this type of VAWT operates primarily through a lift, emphasizing that a higher lift coefficient translates into a higher power coefficient; however, this cost of lift results in the turbines decreasing in self-starting performance. Mohamed *et al.* [22], In their study of the performance improvement of the H-Darrieus rotor, defined $k-\varepsilon$ as the turbulence model. In comparison, with the experimental study of Takahashi *et al.* [23], it was found that the approximate percentage error between the results of the power coefficient was 10.71%, giving reliability in the use of the realizable $k-\varepsilon$ model for this study. The model is typically used for external flows with complex geometry.

A rectangular flow domain with appropriate dimensions is introduced, the rotor radius is 1.25 m, and from the article posted by Raciti, C.M. *et al.* [15]. The inlet and outlet boundary conditions have been adjusted. Table 3 summarises the geometrical characteristics of the VAWT. The domain dimension in width and length, respectively, is between 10 and 20 times the turbine diameter [16]. Figure 4 displays the main dimensions of the control domain.

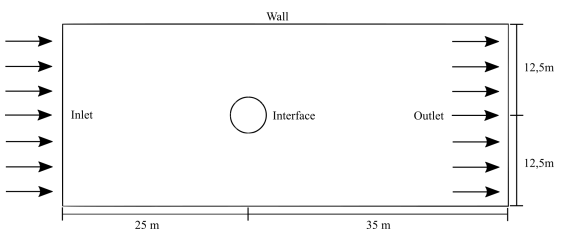

(a) Wind Tunnel sub-grid area

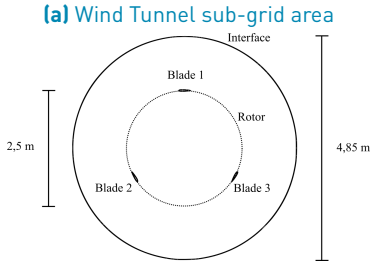

(b) Rotor sub-grid area

Figure 4 Main dimensions of the control domain

The sliding mesh method is used, and the selected grid

Table 2 Summary CFD simulation of the VAWTs

Author	Ferreira et al. [16]	Gupta. R. [17]	Howell, R. et al. [18]	Amet, E. et al. [19]
Dimension	2D	2D	2D,3D	2D
Airfoil	NACA-0015	NACA-0012	NACA-0022	NACA-0018
Diameter D	0.4 m	*	0.3 m	0.12 m
Chord length C	50 mm	50 mm	100 mm	20 mm
Mesh elements	1.6 million	112,450	1.3 million	160,000
Mesh type	Quad	Tri	Tetra	Quad
Domain size	10D*14D	6c	16D	30c
Turbulence model	Standard $k-\varepsilon$	Standard $k-\varepsilon$	RNG $k-\varepsilon$	$k-\omega$
Inlet	Velocity Inlet	Velocity Inlet	Velocity Inlet	Velocity Inlet
Outlet	Pressure outlet	Outflow	Outflow	Pressure Outlet

Table 3 Geometrical characteristics of the VAWT

Parameter	Description
Number of blades, N [m]	3
Diameter, D [m]	2.5
Height, H [m]	1
Solidity, σ[-]	0.3
Airfoil	NACA0015
Airfoil chord, C[m]	0.250
Mounting ratio [-]	0

type is the unstructured grid. An unstructured grid consisting of triangular elements is adopted for both fixed and rotating flow domains. In the vicinity of wall borders, the unstructured grids are significantly increased to obtain a normalized wall distance. It is accomplished using 25 boundary layers with a growth rate of 1.2 for the open Darrieus turbine on all wall surfaces (e.g., the blades). Since the model uses NWT (Near-Wall Treatment) functions, specifically EWT (Enhanced Wall Treatment), a y^+ equal to 30 was defined to avoid conflicts when using NWT for y^+ numbers less than 30. To calculate the height of the first mesh cell off the wall required to achieve the desired y^+ using flat-plate boundary layer theory is given by the Equation (7):

$$y = \frac{y^+ \mu}{\rho u^*} \tag{7}$$

Where y^+ value indicates the wall spacing in (m), dynamic viscosity μ, fluid density ρ, and dimensionless velocity u^*.

The simulation is performed with constant inlet velocity (10 m/s) in all simulations and preserves constant. Both boundary streamlines (e.g., normal derivatives of dependent variables are zero) are subject to symmetry boundary conditions, as seen in Figure 4. The interface boundary condition is used on the circumference of the rotating zone to keep the continuity in the flow field. A non-slip moving is used for the blade surfaces. Figure 5 shows the mesh on the control domain

Five different time-step sizes (10, 5, 2.5, 1, 0.5) have been studied by McLaren [24]. He found that, for the three smallest time-step sizes, the C_p ranges by just 1.5 percent; it is also found that the variation between five steps is not that substantial considering time-saving and reliability issues [24], so the analysis uses 2.5º per time step.

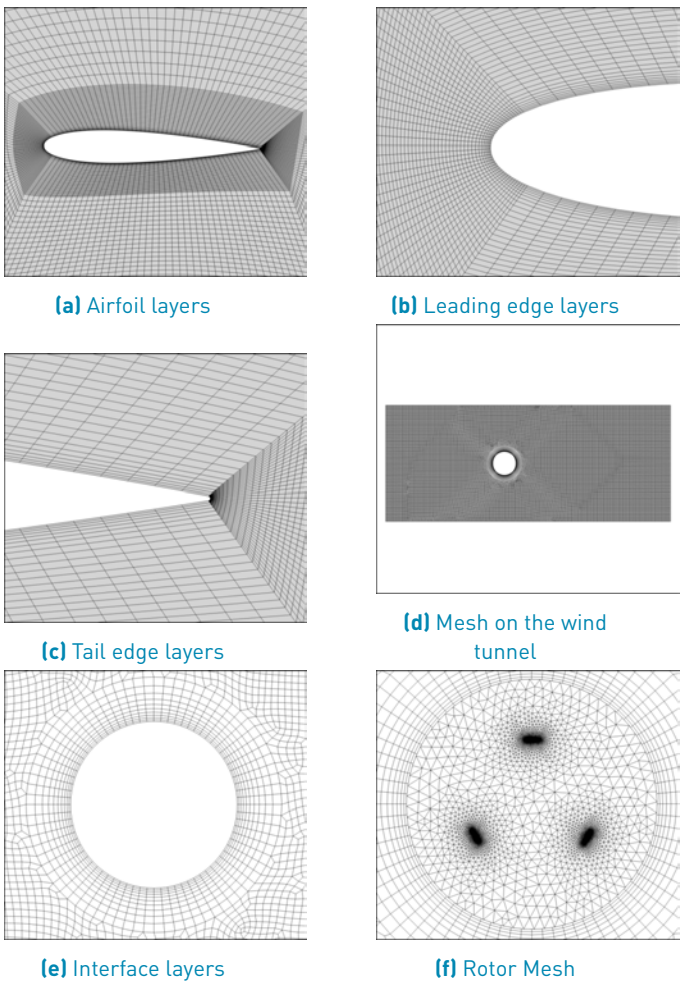

(a) Airfoil layers **(b)** Leading edge layers **(c)** Tail edge layers **(d)** Mesh on the wind tunnel **(e)** Interface layers **(f)** Rotor Mesh

Figure 5 Mesh on the control domain.

Table 4 Grid and boundary conditions

Parameter	Description
Flow domain [m]	Rectangle (60*25)
Interface/Type	Sliding/Conformal
Grid/Type	Unstructed/Tri
Elements	250,000-450,000
Fluid	Air
Turbulence Model	Realizable $\kappa - \epsilon$
Inlet	Velocity Inlet
Outlet	Pressure Outlet
Blades	No-slip moving wall $\omega = 0$ rad/s
Residuals RMS criteria	$1.0x10^{-6}$
Time	Transient
Near-Wall Treatment	Enhanced Wall Treatment (EWT)
$y^+[-]$	30
Freestream velocity ϑ [m/s]	10
Tip speed ratio λ [-]	0 / 0.5 / 1 / 1.5 / 2 / 2.5 / 3 / 4
Time Step Size [s]	0.007
Reynolds Number [-]	1.4E+5

Convergence conditions were established to obtain a periodic variance of the torque coefficient and satisfy a maximum residual value of $1.0x10^{-6}$. Finally, the three-blade torque coefficient was controlled and reported to determine the maximum power coefficient of the Darrieus rotor. Table 4 summarises the grid and boundary conditions. The effect of four turbulence models has been investigated and compiled quantitatively. SST $k-w$ model [25], $k-w$ [26, 27] realizable and standard $k-w$. Figure 6 shows the curves of the four turbulence models proposed. Realizable R was selected due to the model results compared to SST $k-w$ and $k-w$ does not exceed a relative error of 5%, giving reliability for this case. Also, the technique offers good convergence and is not memory-intensive. Based on the CFD strategies,

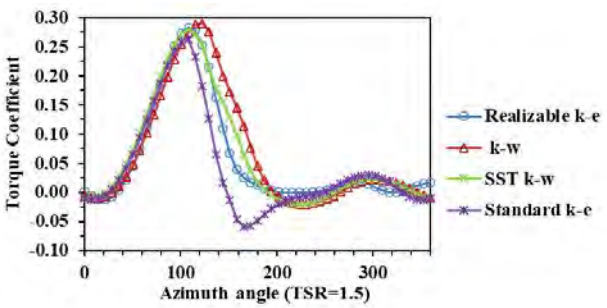

Figure 6 Effect of different turbulence models on the proposed case

this new case was modeled following the experiment performed by McLaren [24] (the model currently used) to validate the simulation results. The comparison between the experimental and simulated results is presented in Figure 7. It is found that the simulation results are positively adapted to the experimental results. However, a remarkable divergence is found for the TSR point equal to 1.5. This divergence may be caused by

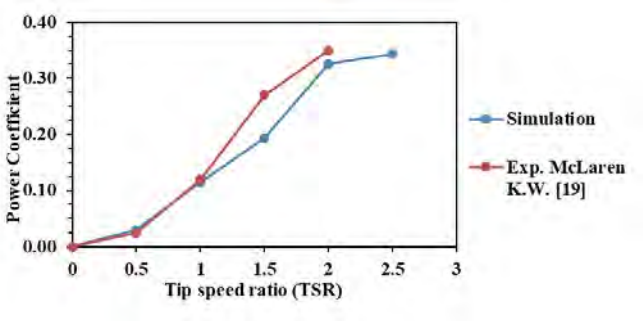

Figure 7 Validation of C_p on the simulated results

the 2D [24] simplification of the 3D model or a possible underestimation of the drag force caused by the turbulence model setup. Despite this, the model has adapted once more when the TSR reaches a value of 2, indicating that the maximum value of C_p is the same as the experimental result.

Additionally, the simulated model shows the same behavior contrasted with the experimental model. The conclusions obtained from this simulation also coincide with the study carried out by Ingham [28], who carried out a CFD mesh independence for the study of a Darrieus rotor. It is highlighted that one way to increase the accuracy of the simulation results is to preserve the conformity of the mesh by avoiding hanging nodes or by using tools provided by the software itself, in the case of ANSYS FLUENT highlighting the use of hanging node adaption because it provides the ability to operate the mesh with variety in the shape of the cell including hybrid meshes. Although this scheme presents excellent flexibility of the mesh, it requires additional memory to maintain the mesh hierarchy used by the rendering and mesh adaptation operations.

4. Simulation results

4.1 The impact of the opening on the C_p as a TSR function

Figure 8 shows how the curves for the C_p work quantitatively with the effect of the opening ratio as a function of TSR. The new model rotor has a diminishing value of maximum C_p as the opening ratio. One possible cause for these reductions is that with the change in the opening ratio, the distance of the trailing edge in the lower surface went forward, which increased the distance region within the airfoil. When the rotor opening ratio is more significant than 0.48, the C_pLP exceeds 30 percent. However, if the opening is a successful option may depend on the overall measurement of more minor C_p losses and a significant C_T improvement.

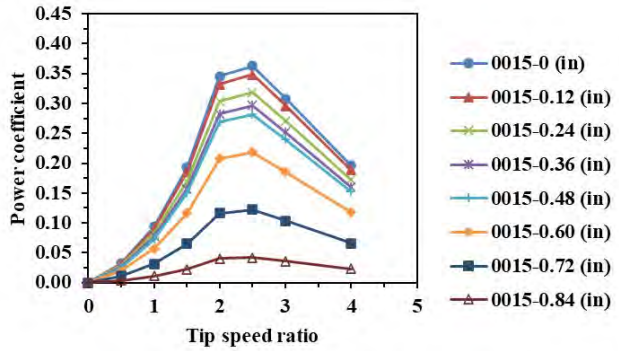

Figure 8 NACA0015 Opening C_p

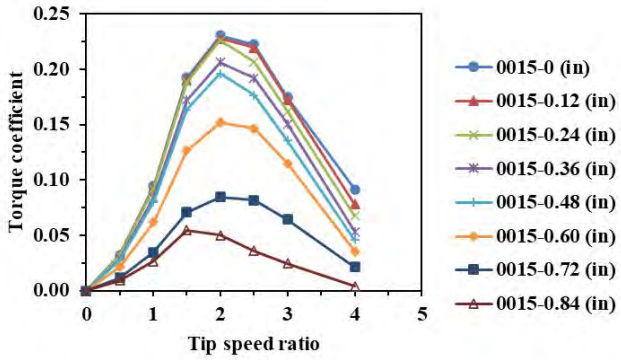

Figure 9 NACA0015 Opening AC_T

Table 5 Maximum Cp of the rotor

Parameter	0015-0 (in)	0015-0.12 (in)	0015-0.24 (in)	0015-0.36 (in)
C_pL	0	3.89	12.29	18.25
MAX	0.3627	0.3486	0.3181	0.2965
TSR	2.5	2.5	2.5	2.5
	0015-0.48 (in)	0015-0.60 (in)	0015-0.72 (in)	0015-0.84 (in)
C_pL	22.30	39.75	66.36	88.33
MAX	0.2818	0.2185	0.1220	0.0423
TSR	2.5	2.5	2.5	2.5

It is also essential to recognize that the power curves of the rotor with the opening are identical to each other while the TSR is less than 1.5. It is maybe because it is not possible to contrast the flow separation induced by the opening with the lower TSR dynamic stall. Nevertheless, the opening flow separation overrides the dynamic stall at high TSR. Another interesting finding in Table 5 is the TSR value of the maximum C_p for all openings when it exceeds 2.5.

4.2 The effect of the opening on the AC_T as a function of TSR

Figure 9 displays rotor curves with various opening ratios AC_T (Average torque coefficient) opening ratios. The AC_T variable structure is relatively similar to the C_p. Notice that the rotors with an opening ratio less than 0.36 present similar C_T at TSR equal to 1.5, which indicates improvement on C_T of the new model. The average AC_T value reduces as the opening ratio increases, unlike the TSR value of the maximum C_p. However, for all rotors, the TSR value for a maximum AC_T is stable, in this case being 2, except for a rotor with an opening ratio of 0.84. This shows that the opening ratio has a slight impact on the overall AC_T TSR value. It is found that the higher opening ratio of the rotor does not indicate a higher AC_T at low TSR. Higher AC_T at low TSR will allow the rotor at low TSR range to pass a standard low solidity Darrieus rotor dead band. Nevertheless, there is no such dead band at a low TSR range for any rotor in this analysis due to the high solidity model.

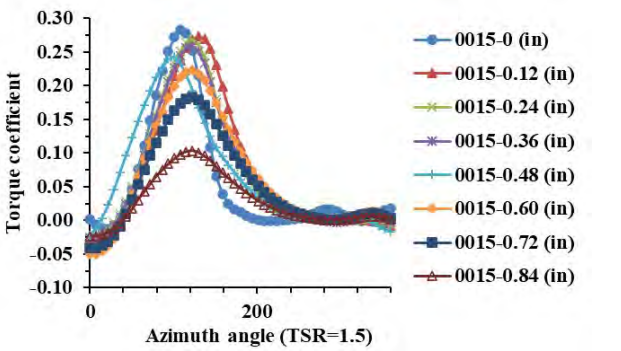

Figure 10 Variation on CT of blade No.1

4.3 The effect of the opening on the C_T as a function of TSR

Figure 10 shows the No.1 blade variation in C_T. The patterns of C_T variability of eight opening ratios in the upwind region at a set TSR are reasonably similar to one another. The average C_T of the eight rotors occurs at the same azimuth angle. It suggests that the opening has a slight impact on the location of maximum C_T. This loss is near the maximum C_T point in the region (45 azimuth angle).

The C_p and C_T would decrease with the growth of the opening ratio. The opening has a reasonably significant adverse impact on C_T in the upwind area. Although there is a positive effect on the C_T in a particular part of the downwind zone, the beneficial impact on the downwind zone is substantially lower than in the upwind zone, thereby lowering the C_T. Figure 11 shows the vorticity magnitude, and Figure 12 shows the velocity magnitude for a TSR of 1.5. It is observed that the velocity decrease in the leading-edge zone is much lower with the opening compared to the airfoil without opening. Because of the opening, the flow does not impact the blade uniformly, and it is also observed that the flow is dispersed in the upwind zone, creating a small vortex that is redirected towards

the opening, causing the flow to enter inside the airfoil opening; as a result of this phenomenon, the airfoil loses some of its velocity and the torque coefficient decreases. This decrease in velocity is accentuated between 180- and 360-degrees azimuth because the airfoil is in the dead zone; however, the airfoil performs optimally between 90- and 180-degrees azimuth because the flow is more uniformly distributed, increasing its velocity.

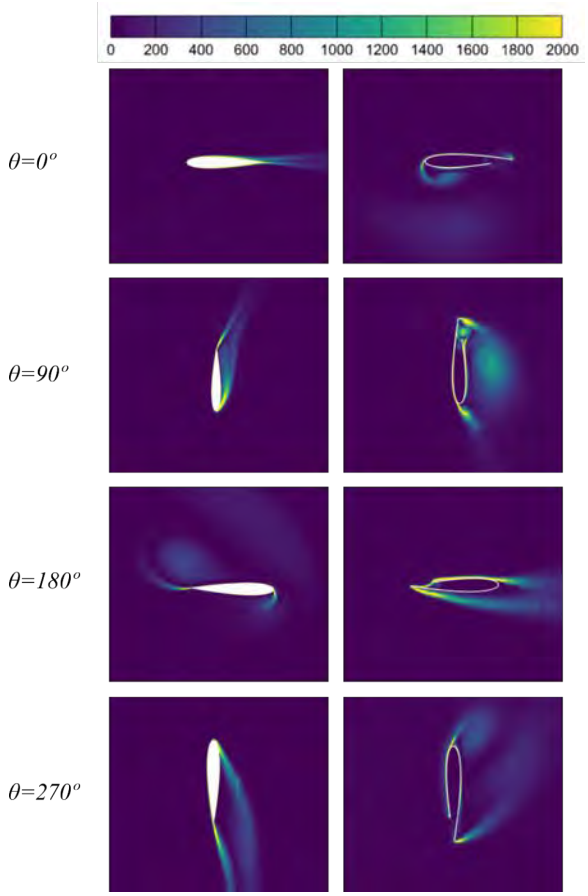

Figure 11 Contour of vorticity magnitude for blade No.1 at TSR=1.5 (inner opening ratio 0 and 0.24)

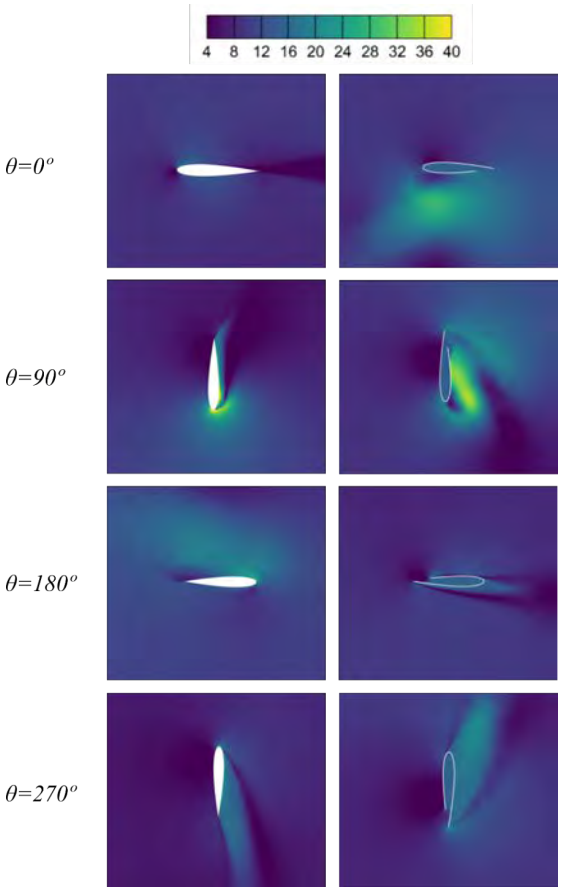

Figure 12 Contour of velocity magnitude for blade No.1 at TSR=1.5 (inner opening ratio 0 and 0.24)

5. Conclusions

The article aims to carry out a thorough analysis of the performance of a new Darrieus rotor type with different opening ratios located on the lower surface. Results have shown that C_PLP increases with an increase in the opening ratio. The C_PLP of the opening rotors ranges from 3.89% to 88.3%. While there is a positive effect on C_T in some downwind zone areas, the positive effect in the downwind region is much smaller than the negative effect in the upwind zone. The positive effect in the downwind zone is much smaller than the negative effect in the upwind zone. As a result, by increasing the opening, the C_T is reduced. Based on the results, the rotors with 0.12 to 0.36 considering the C_PLP, C_T increase, and AC_T increase are the desirable rotors for the opening located at the lower surface.

6. Declaration of competing interest

We declare that we have no significant competing interests, including financial or non-financial, professional, or personal interests interfering with the complete and objective presentation of the work described in this manuscript.

7. Funding

This work was supported by the Instituto Tecnologico Metropolitano.

8. Author contributions

Conceived and designed the analysis: A. Burbano, D. Hincapie, J. Graciano Collected the data: A. Burbano. Contributed data or analysis tools: D. Hincapie J. Graciano, E. Torres and A. Burbano. Performed the analysis: A. Burbano and J. Graciano. Wrote the paper: A. Burbano and E. Torres

9. Data Availability Statement

The project data used to support the findings of this research have been deposlited in the Figshare repository. DOI: https://doi.org/10.6084/m9.figshare.15057294.v2

References

[1] L. Pérez-Lombard, J. Ortiz, and C. Pout, "A review on buildings energy consumption information," *Energy and Buildings*, vol. 40, no. 3, 2008. [Online]. Available: https://doi.org/10.1016/j.enbuild.2007.03.007

[2] US Energy Information Administration, *Annual Energy Outlook 2019 with projections to 2050*. Washington, DC: U.S. Energy Information Administration (EIA), Ene. 24, 2019.

[3] E. Hau, *Wind Turbines: Fundamentals, Technologies, Application, Economics*, 2nd ed. New York: Springer-Verlag Berlin Heidelberg, 2013.

[4] S. Mertens, G. V. Kuik, and G. V. Bussel, "Performance of an H-Darrieus in the Skewed Flow on a Roof," *Journal of Solar Energy Engineering*, vol. 125, no. 4, Nov. 26, 2006. [Online]. Available: https://doi.org/10.1115/1.1629309

[5] I. Hashem and M. H. Mohamed, "Aerodynamic performance enhancements of H-rotor Darrieus wind turbine," *Energy*, vol. 142, no. 19, Ene. 1, 2018. [Online]. Available: https://doi.org/10.1016/j.energy.2017.10.036

[6] A. Fiedler, "The effects of blade pitch and mount point offset on vertical axis wind turbine performance," PhD thesis, McMaster University, Hamilton, Ontario, Canadá, 2009.

[7] P. C. Klimas and M. H. Worstell. (1981, Oct.) Effects of blade preset pitch/offset on curved-blade Darrieus vertical axis wind turbine performance. [Online]. Available: https://www.osti.gov/biblio/5243044

[8] R. H. Liebeck, "Design of subsonic airfoils for high lift," *Journal of Aircraft*, vol. 15, no. 9, Sep. 1970. [Online]. Available: https://doi.org/10.2514/3.58406

[9] D. H. Neuhart and O. C. Pendergraft, *A Water Tunnel Study of Gurney Flaps*. Washington: NASA TM-4071, 1988.

[10] D. Srivastav and K. N. Ponnani, "Surface Modifications for Improved Maneuverability and Performance of an Aircraft," in *ASME 2011 International Mechanical Engineering Congress and Exposition. Volume 1: Advances in Aerospace Technology; Energy Water Nexus; Globalization of Engineering; Posters*. Denver, Colorado: American Society of Mechanical Engineers, 2011, pp. 121–127.

[11] M. F. Ismail and K. Vijayaraghavan, "The effects of aerofoil profile modification on a vertical axis wind turbine performance," *Energy*, vol. 80, Feb. 1, 2015. [Online]. Available: https://doi.org/10.1016/j.energy.2014.11.034

[12] M. R. Castelli, A. Englaro, and E. Benini, "The Darrieus wind turbine: Proposal for a new performance prediction model based on CFD," *Energy*, vol. 36, no. 8, Ago. 2011. [Online]. Available: https://doi.org/10.1016/j.energy.2011.05.036

[13] C. S. Ferreira, G. V. Bussel, and G. V. Kuik, "2D CFD simulation of dynamic stall on a vertical axis wind turbine : verification and validation with PIV measurements," in *45th AIAA Aerospace Sciences Meeting*, Reno, Nevada, 2007, pp. 16 192–16 201.

[14] M. Islam, D. S.-K. Ting, and A. Fartaj, "Aerodynamic models for Darrieus-type straight-bladed vertical axis wind turbines," *Renewable and Sustainable Energy Reviews*, vol. 12, no. 4, May. 2008. [Online]. Available: https://doi.org/10.1016/j.rser.2006.10.023

[15] M. Islam, M. R. Amin, D. S. K. Ting, and A. Fartaj, "Performance Analysis of a Smaller-Capacity Straight-Bladed VAWT with Prospective Airfoils," in *46th AIAA Aerospace Sciences Meeting and Exhibit*, Reno, Nevada, 2008.

[16] F. R. Menter, "Two-equation eddy-viscosity turbulence models for engineering applications," *AIAA Journal*, vol. 32, no. 8, Ago. 1994. [Online]. Available: https://doi.org/10.2514/3.12149

[17] J. Smagorinsky, "General circulation experiments with the primitive equations," *Monthly Weather Review*, vol. 91, no. 3, Mar. 1, 1963. [Online]. Available: https://doi.org/10.1175/1520-0493(1963)091<0099:GCEWTP>2.3.CO;2

[18] W. Szablewski, "B. E. Launder and D. B. Spalding, Mathematical Models of Turbulence. 169 S. m. Abb. London/New York 1972. Academic Press. Preis geb. $ 7,50," *Journal of Applied Mathematics and Mechanics / Zeitschrift für Angewandte Mathematik und Mechanik*, vol. 53, no. 6, 1973. [Online]. Available: https://doi.org/10.1002/zamm.19730530619

[19] K. W. McLaren, "A numerical and experimental study of unsteady loading of high solidity vertical axis wind turbines," PhD thesis, McMaster University, Hamilton, Ontario, Canadá, 2011.

[20] C. Zhang, C. P. Bounds, L. Foster, and M. Uddin, "Turbulence Modeling Effects on the CFD Predictions of Flow over a Detailed Full-Scale Sedan Vehicle," *Fluids*, vol. 4, no. 3, Ago. 1, 2019. [Online]. Available: https://doi.org/10.3390/fluids4030148

[21] P. A. Durbin, "Near-wall turbulence closure modeling without "damping functions"," *Theoretical and Computational Fluid Dynamics*, vol. 3, no. 1, Sep. 1991. [Online]. Available: https://doi.org/10.1007/BF00271513

[22] S. Takahashi, Y. Ohya, T. Karasudani, and K. Watanabe, "Numerical and experimental studies of airfoils suitable for vertical axis wind turbines and an application of wind-energy collecting structure for higher performance," *Journal of Wind Engineering*, vol. 108, 2006. [Online]. Available: https://bit.ly/3ijtSaC

[23] R. Gupta, A. Biswas, and K. K. Sharma, "Comparative study of a three-bucket Savonius rotor with a combined three-bucket Savonius–three-bladed Darrieus rotor," *Renewable Energy*, vol. 33, no. 9, Sep. 2008. [Online]. Available: https://doi.org/10.1016/j.renene.2007.12.008

[24] R. Howell, N. Qin, J. Edwards, and N. Durrani, "Wind tunnel and numerical study of a small vertical axis wind turbine," *Renewable Energy*, vol. 35, no. 2, Feb. 2010. [Online]. Available: https://doi.org/10.1016/j.renene.2009.07.025

[25] E. Amet, T. Maitre, C. Pellone, and J.-L. Achard, "2D Numerical Simulations of Blade-Vortex Interaction in a Darrieus Turbine," *J. Fluids Eng.*, vol. 131, no. 11, Oct. 21, 2009. [Online]. Available: https://doi.org/10.1115/1.4000258

[26] K. M. Almohammadi, D.B.Ingham, L. Ma, and M.Pourkashan, "Computational fluid dynamics (CFD) mesh independency techniques for a straight blade vertical axis wind turbine," *Energy*, vol. 58, Sep. 1, 2013. [Online]. Available: https://doi.org/10.1016/j.energy.2013.06.012

[27] N. Hill, R. Dominy, G. Ingram, and J. Dominy, "Darrieus turbines: The physics of self-starting," *Proceedings of the Institution of Mechanical Engineers, Part A: Journal of Power and Energy*, vol. 223, no. 1, 2009. [Online]. Available: https://doi.org/10.1243/09576509JPE615

[28] R. Dominy, P. Lunt, A. Bickerdyke, and J. Dominy, "Self-starting capability of a Darrieus turbine," *Proceedings of the Institution of Mechanical Engineers, Part A: Journal of Power and Energy*, vol. 221, no. 1, Feb. 1, 2017. [Online]. Available: https://doi.org/10.1243/09576509JPE340